RSC Advances

PAPER

View Article Online
View Journal | View Issue

Cite this: *RSC Adv.*, 2023, **13**, 14530

Application of ZnO-NRs@Ni-foam substrate for electrochemical fingerprint of arsenic detection in water†

Muhammad Rauf,[a] Said Karim Shah, *[a] Ali Algahtani,[bc] Vineet Tirth, [bc] Abdulaziz H. Alghtani,[d] Tawfiq Al-Mughanam,[e] Khizar Hayat, *[a] Nora Hamad Al-Shaalan, [f] Sarah Alharthi, [gh] Saif A. Alharthy[ij] and Mohammed A. Amin[g]

Arsenic (As^{3+}) is the most carcinogenic and abundantly available heavy metal present in the environment. Vertically aligned ZnO nanorod (ZnO-NR) growth was achieved on metallic nickel foam substrate *via* a wet chemical route and it was used as an electrochemical sensor towards As(III) detection in polluted water. Crystal structure confirmation, surface morphology observation and elemental analysis of ZnO-NRs were conducted using X-ray diffraction, field-emission scanning electron microscopy and energy-dispersive X-ray spectroscopy, respectively. Electrochemical sensing performance of ZnO-NRs@Ni-foam electrode/substrate was investigated *via* linear sweep voltammetry, cyclic voltammetry and electrochemical impedance spectroscopy in a carbonate buffer solution of pH = 9 and at different As(III) molar concentrations in solution. Under optimum conditions, the anodic peak current was found proportional to the arsenite concentration from 0.1 μM to 1.0 μM. The achieved values for limit of detection and limit of quantification were 0.046 ppm and 0.14 ppm, respectively, which are far lower than the recommended limits for As(III) detection in drinking water as suggested by the World Health Organization. This suggests that ZnO-NRs@Ni-foam electrode/substrate can be effectively utilized in terms of its electrocatalytic activity towards As^{3+} detection in drinking water.

Received 10th March 2023
Accepted 25th April 2023

DOI: 10.1039/d3ra01574b

rsc.li/rsc-advances

1. Introduction

Arsenic "As(III) or As^{3+}" is the most toxic and widely distributed element among the twenty (20) pollutant elements in the Earth's crust and surprisingly it is the 12th most abundant mineral in the human body.[1,2] Air, water, and food are the main sources through which it gets into the human body.[3] In groundwater, arsenic exists in two different forms, namely arsenate ($HAsO_3^{2-}$, As^{3+}) and arsenite ($HAsO_3^{2-}$, As^{5+}).[4–6] Naturally, arsenic can be found in four different oxidation states, *i.e.*, As^0, As^{3-}, As^{3+}, and As^{5+}, bonded with organic and/or inorganic substances.[7] The most dominant form of arsenic contamination in groundwater is inorganic arsenic which exists in +3 and +5 oxidation states, *i.e.*, As^{3+} and As^{5+}.[8] Furthermore, about 80% toxicity of arsenic is contributed by As^{3+} (ref. 9) which is 50 times more toxic than arsenite due to the fast reactions with enzymes in the human body.[8,10,11] World Health Organization (WHO) and United States Environmental Protection Agency (USEPA) recommended limit for As^{3+} in drinking water is around 10 μg L^{-1}, *i.e.*, 10 ppb.[15–17] Worldwide, different regions affected by arsenic (As^{3+}) contamination include China, India, Bangladesh, Pakistan, Nepal, Thailand, some states like Massachusetts, New Hampshire, Oregon, California, and the seas of the USA and Mexico.[14] Long-term exposure to arsenic causes diverse acute health effects such as bladder cancer, mutagenic effects, genotoxicity, fatigue, hyperkeratosis on feet or palm, cardiovascular events, skin irritation, DNA mutation, and carcinogenesis.[12–14] These health effects depend on the kind of arsenic species existing in a region. Therefore, it is necessary to detect As^{3+} contamination up to the

[a]*Department of Physics, Abdul Wali Khan University Mardan, 23200 Mardan, Khyber Pakhtunkhwa, Pakistan. E-mail: khizar3@awkum.edu.pk; saidkarim@awkum.edu.pk*
[b]*Mechanical Engineering Department, College of Engineering, King Khalid University, Abha 61421, Asir, Kingdom of Saudi Arabia*
[c]*Research Center for Advanced Materials Science (RCAMS), King Khalid University, Guraiger, PO Box 9004, Abha 61413, Asir, Kingdom of Saudi Arabia*
[d]*Department of Mechanical Engineering, College of Engineering, Taif University, PO Box 11099, Taif 21944, Kingdom of Saudi Arabia*
[e]*Department of Mechanical Engineering, College of Engineering, King Faisal University, PO Box 380, Al-Ahsa 31982, Kingdom of Saudi Arabia*
[f]*Department of Chemistry, College of Science, Princess Nourah Bint Abdulrahman University, PO Box 84428, Riyadh 11671, Saudi Arabia*
[g]*Department of Chemistry, College of Science, Taif University, PO Box 11099, Taif 21944, Saudi Arabia*
[h]*Center of Advanced Research in Science and Technology, Taif University, PO Box 11099, Taif 21944, Saudi Arabia*
[i]*Department of Medical Laboratory Sciences, Faculty of Applied Medical Sciences, King Abdulaziz University, PO Box 80216, Jeddah 21589, Saudi Arabia*
[j]*King Fahd Medical Research Center, King Abdulaziz University, PO Box 80216, Jeddah 21589, Saudi Arabia*

† Electronic supplementary information (ESI) available. See DOI: https://doi.org/10.1039/d3ra01574b

aforementioned concentration limit in both biological and environmental fields.[18–20] In the last few decades several analytical approaches have been followed for arsenic detection including liquid chromatography,[21–23] mass spectrometry,[24] inductively coupled plasma-mass spectrometry,[25] liquid chromatography,[26] surface-enhanced Raman spectrometry, graphite furnace atomic absorption spectrometry,[27] ozone gas-phase chemiluminescence,[28] electrochemical detection,[29] *etc.* All these techniques have pronounced sensitivity and excellent limits of detection. However, some limitations such as expensive instruments or laboratory setup, control difficulty, large consumption of organic substances, and time-consuming procedures hinder the potential uses of these techniques.[14,18] Consequently, an onsite, rapid and simple analytical ultrasensitive technique is needed to develop qualitative as well as quantitative detection of arsenic in samples.[30] In contrast to these conventional analytical techniques, an electrochemical approach is the most convenient and effective route to detect quite easily various arsenic concentrations in samples. Formerly, different electrochemical techniques have commonly been utilized such as linear sweep anodic stripping voltammetry (LSASV), cathodic stripping voltammetry (CSV), linear sweep voltammetry (LSV), differential pulse anodic stripping voltammetry (DPSAV), electrochemical impedance spectroscopy (EIS), and cyclic voltammetry (CV)[31,32] which can also differentiate various oxidation states of arsenic in pollutants. Similarly, to enhance the analytical sensitivity for arsenic detection, some research groups have tried to modify the surface of working electrodes in the aforesaid techniques by decorating them with different nanomaterials such as Au, C–Au nanoparticles (NPs), Pt, Si, ZnO quantum dots,[1,6,33–36] *etc.* Besides these nanomaterials various nanocomposites have been also reported for arsenic detection such as Au–Pt NPs/PANI, boron-doped diamond (BBD), and Au-Ppy NWs.[14,29,37] Zinc oxide (ZnO) is a II–IV semiconductor compound with a direct band gap of ~3.37 eV and maximum exciton binding energy of ~60 meV at ambient temperature and has been extensively reported in various fields such as photoelectrical applications,[38–41] photocatalytic applications,[42,43] antibacterial activity towards pathogenic bacteria for medical application,[44,45] transparent electrode for solar cell, low band gap in optoelectronic devices[46–48] *etc.* Besides its physicochemical characteristics, ZnO reveals environmental advantages like non-toxicity, easy disposal of materials, recyclability, and corrosion resistance. Based on these characteristics, ZnO can be assumed to be a green material for environmental engineering applications.[49]

In the present work, ZnO nanorod vertical growth on analytical-grade pure nickel (Ni) foam *via* a wet electrochemical route is optimized. Crystal structure, surface morphology observation, and elemental analysis were conducted using XRD, FESEM, and EDS, respectively. ZnO-NRs@Ni-foam was then used as a working electrode in electrochemical measurements for detecting As^{3+} in aqueous media. CV, LSV and EIS measurements of ZnO-NRs@Ni-foam electrode in carbonate buffer solution (CBS, pH = 9) with various As(III) concentrations were made which showed high catalytic activity of ZnO-NRs@Ni-foam electrode/substrate towards arsenic detection.

2. Experimental section

2.1. Reagents

Zinc acetate dihydrate ($Zn(CH_3COO)_2 \cdot 2H_2O$, purity > 99%, Sigma-Aldrich), zinc nitrate hexahydrate ($Zn(NO_3)_2 \cdot 6H_2O$, 98.0%, Sigma-Aldrich), sodium hydroxide (NaOH, purity > 97%, Sigma), ammonium hydroxide (NH_4OH, 32%, Merck), CBS (pH = 9), concentrated As(III) solution, absolute ethanol, hydrochloric acid (HCl), high-purity nickel foam (~95% porous), and deionized (DI) water were used as starting materials for the growth of ZnO nanorods on highly porous nickel foam substrate. All these reagents were of analytical grade and were used without further purification.

2.2. Characterization techniques

An X-ray diffractometer (Philips PW 1729) with CuKα1 radiation (λ = 1.5406 Å) was used to analyze the crystal structure of ZnO nanorods grown on Ni-foam substrate. Field-emission scanning electron microscopy (FESEM; Zeiss LEO 1550 Gemini) was employed to observe the surface morphology of samples. Elemental analysis was carried out with an energy-dispersive X-ray spectrometer (EDS) attached to the FESEM system. Electrochemical performances of ZnO-NR-based Ni-foam electrodes/substrates were investigated *via* a three-electrode electrochemical workstation (CHI potentiostat, USA). ZnO-NRs@Ni-foam, platinum plate and Ag/AgCl were used as working electrode, counter electrode, and reference electrode, respectively.

2.3. Growth methodology

Firstly, Ni-foam surfaces were cleaned thoroughly with dilute HCl, ethanol and then DI water in an ultrasonic bath each for ~15 minutes followed by drying in a vacuum oven. Zinc acetate solution (0.1 M) was prepared in DI water. Clean Ni-foam substrate was immersed a few times in zinc acetate solution and then dried in an oven at 150 °C for 2 h to grow ZnO seed layer to produce a favourable condition for uniform vertical ZnO nanorod growth on Ni-foam surfaces. For ZnO-NR growth, $Zn(NO_3)_2 \cdot 6H_2O$ solution (0.1 M, 100 ml) was prepared in DI water. 3.5 mL NH_3 (aq.) was added dropwise to this solution and then vigorously stirred for a further 30 min to get the final growth solution. ZnO seed layer-grown Ni-foam was then fixed horizontally in a Teflon holder inside a glass beaker containing the growth solution as shown schematically in Fig. 1. Ni-foam was held about 1 cm below the growth solution surface to eliminate contamination. It was wrapped with aluminium foil and kept in an oven at 95 °C for 6 hours to grow ZnO nanorods. After the growth process, Ni-foam was thoroughly cleaned with DI water and dried at 100 °C for 2 hours. The whole synthesis procedure is summarized schematically in Fig. 1.

3. Results and discussion

3.1. Structural analysis

The crystallinity and phase purity of ZnO-NRs@Ni-foam were examined through X-ray diffraction (XRD) analysis. Fig. 2(a)

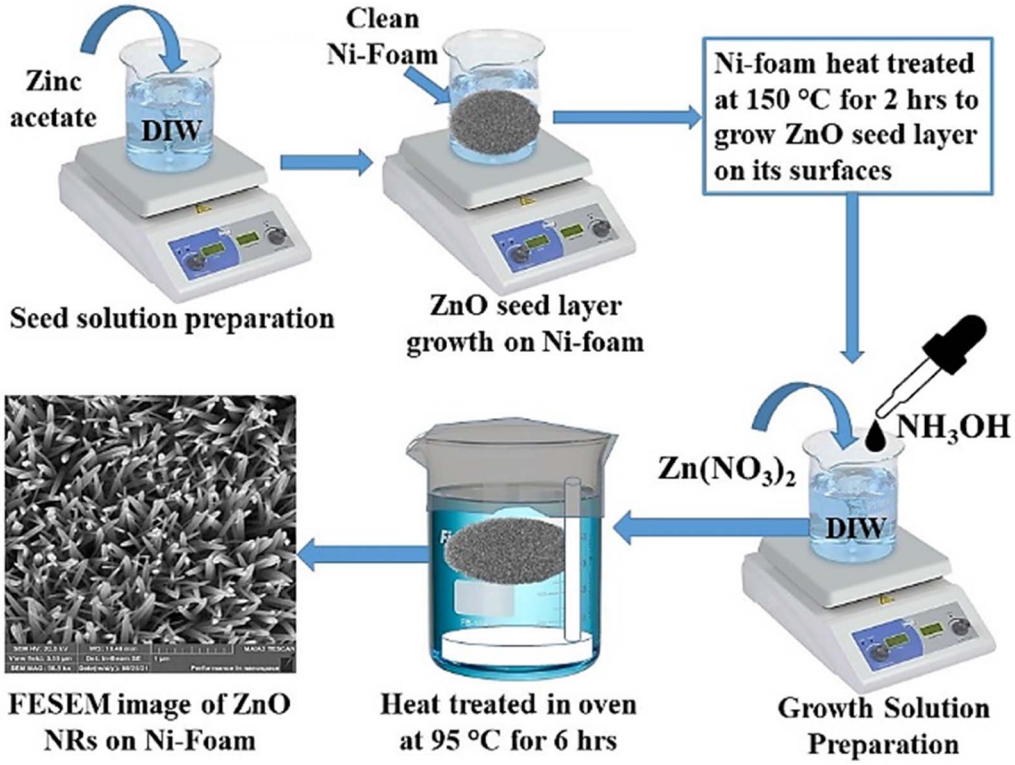

Fig. 1 Schematic representation ZnO-NR growth on Ni-foam substrate.

shows the XRD pattern of bare Ni-foam before growth, recorded from 20° to 80°. The diffraction peaks at 38.3°, 52.2°, and 77.21° match well with JCPDS card #03-1051. Fig. 2(b) shows the XRD pattern of ZnO-NRs@Ni-foam electrode. The diffraction peaks marked by asterisks (*) at 2θ positions of 38.47°, 44.74°, 65.14° and 78.2° are due to the aluminium substrate used. These diffraction peaks matched well with standard XRD data of aluminium powder from JCPDS card #04-0787. While the diffraction peaks located at 2θ positions around 32.2°, 34.9°, 65.5°, 48.0°, 65.5°, 63.1°, *etc.* are due to the hexagonal wurtzite structure of ZnO nanorods grown on nickel foam surfaces. All these peaks were indexed using ZnO standard powder XRD data with JCPDS card #01-079-0205. The XRD pattern confirmed the single-phase formation of ZnO nanorods on Ni-foam.

3.2. Morphological analysis

Surface morphology of ZnO-NRs@Ni-foam was examined *via* FESEM. Fig. 3(a) shows the FESEM image of bare Ni-foam before growth while Fig. 3(b) shows that after growth. Fig. 3(c) shows a high magnification FESEM image of ZnO-NRs grown on Ni-foam which reveals highly uniform and vertically aligned growth of ZnO nanorods on Ni-foam covering all outer and inner surfaces. Elemental analysis of as-prepared ZnO-NRs was carried out *via* EDS attached to the FESEM system. Fig. 3(d) shows the EDS pattern of ZnO-NRs recorded on Ni-foam. In the EDS spectrum, the three peaks at ~1.016, 8.62, and 9.54 keV denoted by symbol "Zn" are due to characteristic different shell transitions.[50,51] The two small-intensity Ni peaks around 7.5 and

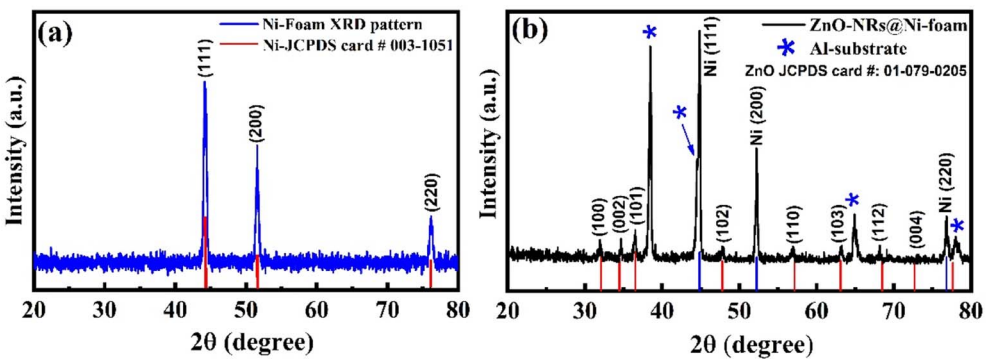

Fig. 2 X-ray diffraction patterns of (a) Ni-foam and (b) ZnO-NRs grown on Ni-foam.

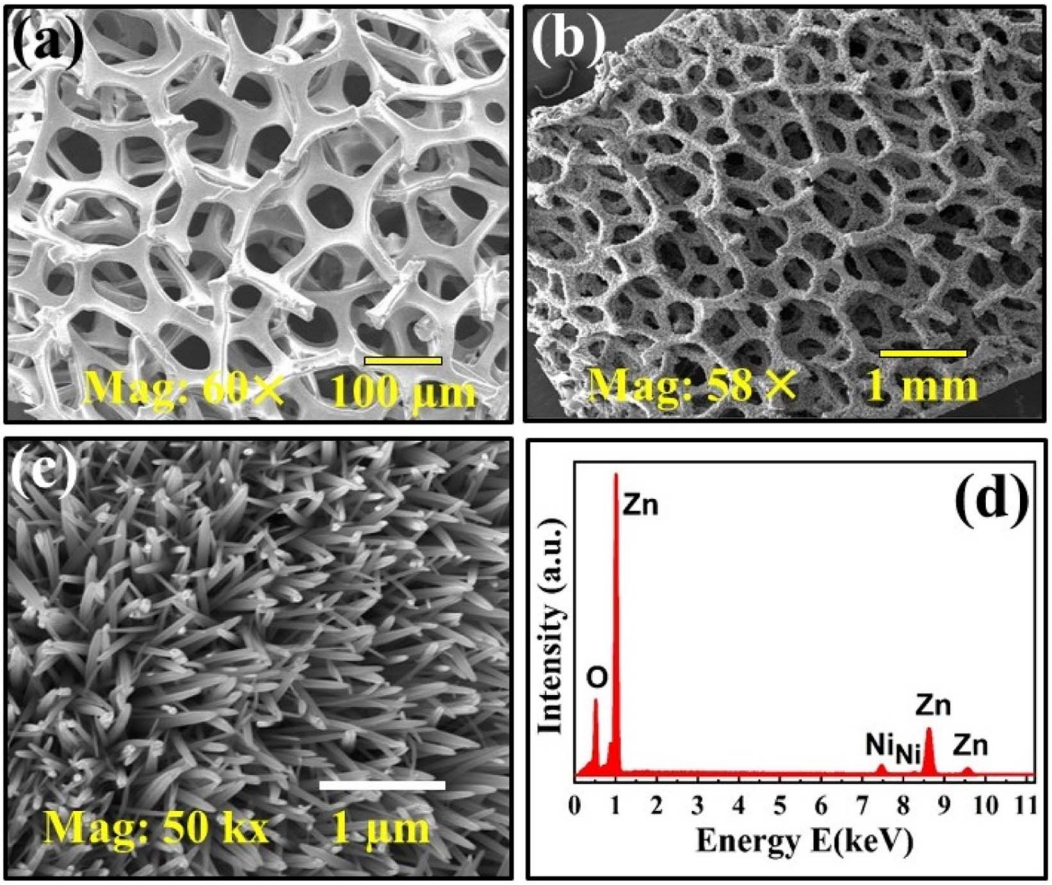

Fig. 3 FESEM micrographs of Ni-foam (a) before growth and (b) after growth. (c) High-resolution image of ZnO nanorods grown on Ni-foam surfaces. (d) EDS spectrum of ZnO-NRs@Ni-foam.

8.2 keV are due to the Ni substrate used. No obvious characteristic impurity peak can be observed, which suggests the formation of highly pure ZnO-NRs on Ni-foam, strongly supporting the XRD results.

3.3. Electrochemical analysis

3.3.1. Cyclic voltammetry analysis. CV measurements of bare Ni-foam and ZnO-NRs@Ni-substrate were carried at an operational potential window ranging from 0 to 1.0 V (*vs.* Ag/AgCl) at a scan rate of 50 mV s^{-1} in CBS (pH = 9) and concentrated As(III) solution at different concentrations. The oxidation and reduction reaction at the working electrode surface is shown in the CV profile in Fig. 4(a). The CV profiles in CBS for bare Ni-foam and ZnO-NRs@Ni-foam show a small faradaic current by the former at ~0.99 V which confirms that ZnO-NRs do not have a catalytic response towards the carbonate.

The CV curve shown in black in Fig. 4(b) reveals the As(III) electrocatalytic activity of bare Ni-foam electrode in 1 μM solution of $NaAsO_2$. A value of 0.124 μA was achieved for anodic peak current at 0.99 V which confirms a minimum electrochemical response. However, a strong rising faradaic current of ~0.394 μA was achieved at 0.99 V for ZnO-NRs@Ni-foam electrode in the same 0.1 μM solution of $NaAsO_2$. This indicates the catalytic activity of the ZnO-NRs@Ni-foam electrode towards As(III) oxidation which is substantially maximum as compared to the bare Ni-foam. Furthermore, the effect of As(III) concentration on the ZnO-NRs@Ni-foam electrode was investigated by varying the electrolyte molarity such as 0.1, 0.2, 0.4, 0.6, 0.8, and 1.0 μM. It is obvious from Fig. 4(c) that the anodic peak current increases with increasing As(III) concentration in the electrolyte. A maximum anodic peak current of ~0.761 μA was achieved at a voltage of ~0.998 V in 1.0 μM concentration. For further quantitative analysis, limit of detection (LOD) and limit of quantification (LOQ) were evaluated (Table 1). LOD is the sample limit to detect the minimum amount of analyte while LOQ is the lowest amount of quantitative analyte measurement in a sample with reasonable accuracy and precision.[8] LOD and LOQ for investigating the ZnO-NRs@Ni-foam electrode were calculated using following eqn (1) and (2):

$$\mathrm{LOD} = \frac{3.3S_b}{m} \quad (1)$$

$$\mathrm{LOQ} = \frac{10S_b}{m} \quad (2)$$

where S_b is the standard deviation and m is the slope of the calibration curve of current *vs.* concentration. From eqn (1) and (2), the calculated LOD and LOQ values for the ZnO-NRs@Ni-foam electrode are 0.046 ppm and 0.14 ppm, respectively.

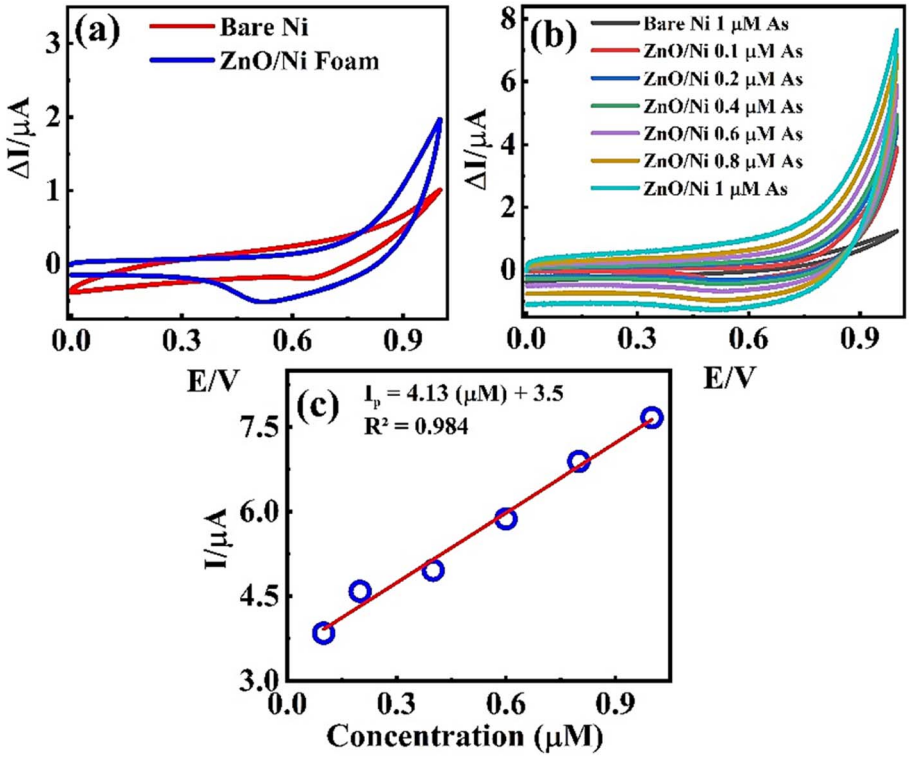

Fig. 4 (a) CV curves of bare Ni-foam and ZnO-NRs@Ni-foam electrode in CBS solution. (b) CV curves of ZnO-NRs@Ni-foam in As(III) solution having different molarity. (c) Regression plot of faradaic current *vs.* concentration.

These values are slightly lower than the WHO recommended limit for As(III) in drinking water which is attributed to the electrocatalytic activity of ZnO-NRs towards As^{3+} detection.[15–17]

3.3.2. Electrochemical impedance spectroscopy analysis. EIS tests in CBS and 1.0 μM As^{3+} solution were carried out to further investigate the interfacial characteristics of ZnO-NRs@Ni-foam as working electrode. Fig. 5(a) reveals the Nyquist plots of bare Ni foam in CBS and 1.0 μM As^{3+} solution. Each EIS spectrum consists of two low- and high-frequency regions. In the high-frequency region, the area of the semi-circle corresponds to the charge transfer resistance R_{ct}. The solution resistance R_S can be measured from the real axis intercept of the Nyquist plot. The low-frequency region (linear part) of EIS spectra indicates the Warburg impedance W_d associated with analyte diffusion through the working electrode. The R_S values of bare Ni-foam and ZnO-NRs@Ni-foam electrodes are found to be 1.87 Ω and 41 Ω, respectively, in As^{3+} solution of 1.0 μM. Nyquist plots of the ZnO-NRs@Ni-foam electrode in Fig. 5(b) demonstrate an obvious reduction in R_{ct} value, *i.e.*, 4.78 Ω, as compared to the bare Ni-foam electrode, *i.e.*, 75.71 Ω. This significant decrease in R_{ct} is due to resultant modification of Ni-foam surface with vertical growth of ZnO-NRs on it. This modification contributes to the improvement of electron transfer kinematics and the excellent electrocatalytic response towards arsenic detection.

3.3.3. Linear sweep voltammetry analysis. LSV was performed to further investigate the sensing response/performance of both bare Ni-foam and ZnO-NRs@Ni-foam electrodes using CBS and different As(III) concentrations. For LSV measurement, a potential window ranging from −0.2 to +0.9 V was selected as shown in Fig. 6(a)–(c). Fig. 6(a) shows the LSV of bare Ni-foam in CBS (pH = 9) and As(III) solution of 1.0 μM. Bare electrode shows

Table 1 A comparative analysis of present and previously reported work

Material	As(III) concentration	LOD (ppb)	Ref.
ZnO-NRs@Ni-foam	0.1–1.0 μM	0.046	Present work
ZnO/NPG microelectrode	1.0–260 ppb	0.3	52
ZnO–GO nanocomposite	80 μM	0.24 μM	53
ZnO quantum dots	10–100 ppb (fluorescent)	7	54
Au modified GCE	0.9–38.99 ppb	0.72	55
Au modified screen printed electrode	0.075–30 μg L^{-1}	0.11 ppb (μg L^{-1})	56
DWCNTs and Gr hybrid thin film	1–10 ppb	0.287	57
$SrTiO_3$/β-CD/GC electrode	10–140 μM	0.02	58
Si NPs/Au-NPs composite	10–100 ppb	5.6 ppb	59

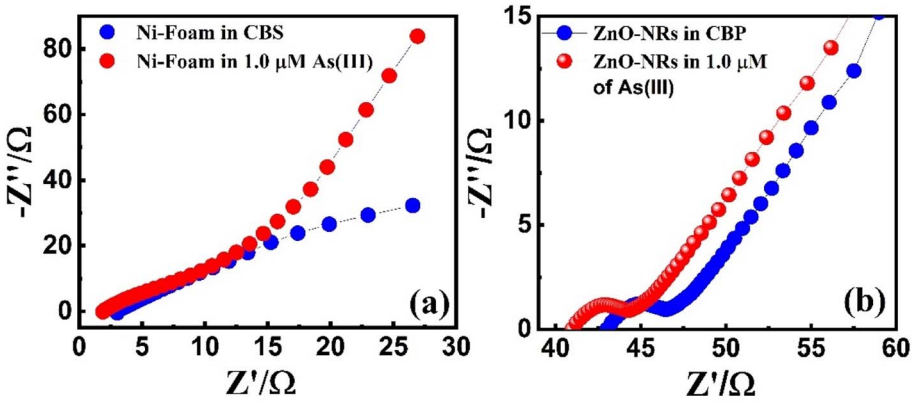

Fig. 5 Nyquist plots of (a) bare Ni-foam and (b) ZnO-NRs@Ni-foam tested in CBS and 1.0 μM As(III) solution.

a negligible catalytic effect in CBS (pH = 9) and creates a small current of ~0.106 μA at a potential of 0.79 V in As^{3+} solution of 1.0 μM. This indicates a poor performance of bare Ni-foam towards As^{3+} detection. Similarly, the electrocatalytic activity of the ZnO-NRs@Ni-foam electrode was characterized in both CBS and arsenic solution of different molarity ranging from 0.1 μM to 1.0 μM. In CBS, the ZnO-NRs@Ni-foam electrode shows a substantially high current of ~0.207 μA at 1.0 V indicating high catalytic activity of the ZnO-NRs@Ni-foam electrode. Furthermore, ZnO-NRs@Ni-foam indicates a stripping current of ~0.368 mA at 0.8 V at 0.1 μM, which reveals that the ZnO-NRs@Ni-foam electrode has a maximum response as compared to bare Ni-foam. The stripping current of the ZnO-NRs@Ni-foam electrode was found to increase with increasing As^{3+} concentration. This indicates that ZnO-NRs on Ni-foam surfaces respond actively and efficiently to positively charged analyte. Likewise, LOD and LOQ of the ZnO-NRs@Ni-foam electrode were determined using eqn (1) and (2). Corresponding LOD and LOQ values are 0.028 ppm and 0.085 ppm, respectively, which are far less than the WHO recommended values. These findings showed that As(III) in aqueous media has been efficiently detected by our design of ZnO-NRs@Ni-foam electrode even at a very low arsenic concentration followed by safe LOD and LOQ values as recommended by WHO. Thus, the ZnO-NRs@Ni-foam electrode can find potential application for electrochemical fingerprint detection of arsenite in pollutant water.[15–17]

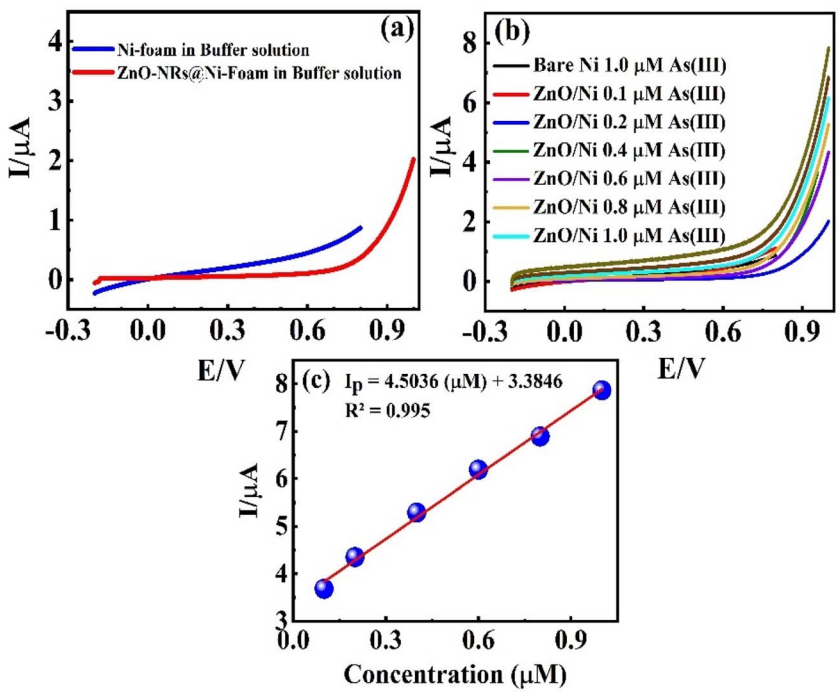

Fig. 6 LSV curves of bare Ni-foam and ZnO-NRs@Ni-foam in (a) CBS and (b) As(III) solution with different concentration. (c) Regression plot of faradaic current *vs.* concentration.

4. Conclusion

A wet chemical route was employed to grow successfully ZnO-NRs on Ni-foam surfaces. XRD results confirmed ZnO single-phase formation with hexagonal wurtzite structure. FESEM micrographs showed well-aligned uniform vertically dense growth of ZnO nanorods on nickel foam surfaces. EDS results also confirmed the formation of ZnO on the surfaces of nickel foam. Electrocatalytic characterization techniques such as CV, EIS, and LSV of bare Ni-foam and ZnO-NRs@Ni-foam electrode/substrate towards pollutant As(III) detection were carried out in CBS with optimum pH = 9 and different As(III) concentration. CV results revealed that the ZnO-NRs@Ni-foam electrode exhibited a substantially high electrocatalytic response (*i.e.*, achieved anodic peak current of 0.124 μA at 0.99 V) towards the oxidation of As(III) as compared to bare Ni-foam. The EIS measurements revealed that the presence of ZnO-NRs@Ni-foam substrate effectively reduced the charge transfer resistance and promoted the electron transfer kinetics. Regression curve of CV measurements was used to calculate the LOD and LOQ for the ZnO-NRs@Ni-foam electrode. Obtained values of LOD and LOQ are 0.046 ppm and 0.14 ppm, respectively. Similarly, LOD and LOQ values obtained from LSV results are 0.028 ppm and 0.085 ppm, respectively. Both these results reveal that the LOD and LOQ values are far less than the WHO recommended concentration of As^{3+} in drinking water. These findings suggested that ZnO-NRs@Ni-foam electrode/substrate can be used effectively as an electrochemical sensor towards the detection of hazardous As^{3+}.

Author contributions

All authors contributed equally to the article in conceptualization, investigation, analysis, writing original draft, review and editing.

Conflicts of interest

The authors declare no conflict of interest.

Acknowledgements

The authors extend their appreciation to the Deanship of Scientific Research at King Khalid University, Abha 61421, Asir, Kingdom of Saudi Arabia for funding this work through the Large Groups Project under grant number RGP.2/142/44. The authors acknowledge the Deanship of Scientific Research, Vice Presidency for Graduate Studies and Scientific Research at King Faisal University, Saudi Arabia, for financial support under the annual funding track [GRANT3378]. The authors also would like to thank Princess Nourah Bint Abdulrahman University Researchers Supporting Project (number PNURSP2023R9), Princess Nourah Bint Abdulrahman University, Riyadh, Saudi Arabia for supporting this project.

References

1 D. A. Quang, D. M. Nguyen and T. T. T. Toan, Determination of arsenic(III) in water using gold nanorods-modified electrode, *J. Mater. Sci.: Mater.*, 2021, 1–13.
2 R. S. Salunke, P. G. Chavan and D. J. Shirale, Anodic stripping voltammetry studies of electrochemically engineered silver nanoparticles over single polypyrrole nanowire device for tracing of arsenic(III): an environmental perspective, *Nanotechnol. Environ. Eng.*, 2018, **3**(1), 1–8.
3 E. Majid, S. Hrapovic, Y. Liu, K. B. Male and J. H. J. Luong, Electrochemical determination of arsenite using a gold nanoparticle modified glassy carbon electrode and flow analysis, *Anal. Chem.*, 2006, **78**(3), 762–769.
4 B. K. Jena and C. R. Raj, Gold nanoelectrode ensembles for the simultaneous electrochemical detection of ultratrace arsenic, mercury, and copper, *Anal. Chem.*, 2008, **80**(13), 4836–4844.
5 B. Ren, P. Sudarsanam, A. E. Kandjani, B. Hillary, M. H. Amin, S. K. Bhargava and L. A. Jones, Electrochemical Detection of As(III) on a Manganese Oxide–Ceria (Mn_2O_3/CeO_2) Nanocube Modified Au Electrode, *Electroanalysis*, 2018, **30**(5), 928–936.
6 S. Ismail, N. A. Yusof, J. Abdullah and S. F. A. Rahman, Electrochemical Detection of Arsenite Using a Silica Nanoparticles-Modified Screen-Printed Carbon Electrode, *Materials*, 2020, **13**(14), 3168.
7 Y.-H. Yuan, X.-H. Zhu, S.-H. Wen, R.-P. Liang, L. Zhang and J.-D. Qiu, Electrochemical assay for As(III) by combination of highly thiol-rich trithiocyanuric acid and conductive reduced graphene oxide nanocomposites, *J. Electroanal. Chem.*, 2018, **814**, 97–103.
8 A. S. Agnihotri, A. Varghese and M. Nidhin, Ion-imprinted chitosan-stabilized biogenic silver nanoparticles for the electrochemical detection of arsenic(III) in water samples, *New J. Chem.*, 2023, **47**, 5179–5192.
9 L. Bu, J. Liu, Q. Xie and S. Yao, Anodic stripping voltammetric analysis of trace arsenic(III) enhanced by mild hydrogen-evolution at a bimetallic Au–Pt nanoparticle modified glassy carbon electrode, *Electrochem. Commun.*, 2015, **59**, 28–31.
10 B. K. Mandal and K. T. Suzuki, Arsenic round the world: a review, *Talanta*, 2002, **58**(1), 201–235.
11 W. H. Organization, *Water, Sanitation, Hygiene And Health: A Primer For Health Professionals*, World Health Organization, 2019.
12 T. Feng, K. Chen, J. Zhong, Y. Cheng, H. Zhao and M. Lan, *In situ* polymerization of dendritic polyaniline nanofibers network embedded with Ag@ SiO_2 core–shell nanoparticles for electrochemical determination of trace arsenic(III), *Sens. Actuators, B.*, 2022, **369**, 132265.
13 R. MacDonald, *Providing Clean Water: Lessons from Bangladesh: Large Parts of the World Face an Unwelcome Choice Between Arsenic and Micro-Organisms*, British Medical Journal Publishing Group: BMJ, 2001.

14 L. M. Camacho, M. Gutiérrez, M. T. Alarcón-Herrera, M. de Lourdes Villalba and S. J. C. Deng, Occurrence and treatment of arsenic in groundwater and soil in northern Mexico and southwestern USA, *Chemosphere*, 2011, **83**(3), 211–225.

15 G. Melinte, O. Hosu, M. Lettieri, C. Cristea and G. Marrazza, Electrochemical fingerprint of arsenic(III) by using hybrid nanocomposite-based platforms, *Sensors*, 2019, **19**(10), 2279.

16 N. Moghimi, M. Mohapatra and K. T. Leung, Bimetallic nanoparticles for arsenic detection, *Anal. Chem.*, 2015, **87**(11), 5546–5552.

17 P. Roy and A. Saha, Metabolism and toxicity of arsenic: A human carcinogen, *Curr. Sci.*, 2002, 38–45.

18 B. M. Sonkoue, P. M. S. Tchekwagep, C. P. Nanseu-Njiki and E. Ngameni, Electrochemical determination of arsenic using silver nanoparticles, *Electroanalysis*, 2018, **30**(11), 2738–2743.

19 F. Pereira, M. Vázquez, L. Debán and A. Aller, Cyclic voltammetry of arsenic-doped cysteine-capped ceramic nanoparticles, *Electrochim. Acta.*, 2013, **109**, 125–135.

20 X.-j. Li, C.-s. Liu, F.-b. Li, Y.-t. Li, L.-j. Zhang, C.-p. Liu and Y.-z. Zhou, The oxidative transformation of sodium arsenite at the interface of α-MnO_2 and water, *J. Hazard. Mater.*, 2010, **173**(1–3), 675–681.

21 G. Tremiliosi-Filho, L. Dall'Antonia and G. Jerkiewicz, Growth of surface oxides on gold electrodes under well-defined potential, time and temperature conditions, *J. Electroanal. Chem.*, 2005, **578**(1), 1–8.

22 R. Sitko, P. Janik, B. Zawisza, E. Talik, E. Margui and I. Queralt, Green approach for ultratrace determination of divalent metal ions and arsenic species using total-reflection X-ray fluorescence spectrometry and mercapto-modified graphene oxide nanosheets as a novel adsorbent, *Anal. Chem.*, 2015, **87**(6), 3535–3542.

23 Q. Liu, H. Peng, X. Lu and X. C. Le, Enzyme-assisted extraction and liquid chromatography mass spectrometry for the determination of arsenic species in chicken meat, *Anal. Chim. Acta*, 2015, **888**, 1–9.

24 I. M. Hwang, H. M. Lee, H.-W. Lee, J.-H. Jung, E. W. Moon, N. Khan and S. H. Kim, Determination of Toxic Elements and Arsenic Species in Salted Foods and Sea Salt by ICP-MS and HPLC-ICP-MS, *ACS Omega*, 2021, **6**(30), 19427–19434.

25 S. Kara, D. S. Chormey, A. Saygılar and S. Bakırdere, Arsenic speciation in rice samples for trace level determination by high performance liquid chromatography-inductively coupled plasma-mass spectrometry, *Food Chem.*, 2021, **356**, 129706.

26 H. Tang, C. Zhu, G. Meng and N. Wu, Surface-enhanced Raman scattering sensors for food safety and environmental monitoring, *J. Electrochem. Soc.*, 2018, **165**(8), B3098.

27 K. Fujiwara, H. Tsubota and T. Kumamaru, Ozone gas-phase chemiluminescence detection of arsenic, phosphorus, and boron in environmental waters, *Anal. Sci.*, 1991, **7**(Suppl.), 1085–1086.

28 T. Agustiany, M. Khalil, Y. Einaga, P. K. Jiwanti and T. A. Ivandini, Physics, Stable iridium-modified boron-doped diamond electrode for the application in electrochemical detection of arsenic(III), *Mater. Chem. Phys.*, 2020, **244**, 122723.

29 A. P. M. Udayan, B. Kachwala, K. Karthikeyan and S. Gunasekaran, Ultrathin quasi-hexagonal gold nanostructures for sensing arsenic in tap water, *RSC Adv.*, 2020, **10**(34), 20211–20221.

30 D. Q. Hung, O. Nekrassova and R. G. Compton, Analytical methods for inorganic arsenic in water: a review, *Talanta*, 2004, **64**(2), 269–277.

31 Z. Guo, M. Yang and X.-J. Huang, Recent developments in electrochemical determination of arsenic, *Environ. Chem.*, 2017, **3**(1), 130–136.

32 W. Ma, Q. Chang, J. Zhao and B.-C. Ye, Novel electrochemical sensing platform based on ion imprinted polymer with nanoporous gold for ultrasensitive and selective determination of As^{3+}, *Microchim. Acta*, 2020, **187**(10), 1–9.

33 T. Mushiana, N. Mabuba, A. O. Idris, G. M. Peleyeju, B. O. Orimolade, D. Nkosi, R. F. Ajayi, O. A. J. S. Arotiba and B.-S. Research, An aptasensor for arsenic on a carbon-gold bi-nanoparticle platform, *Sens. Bio-Sens. Res.*, 2019, **24**, 100280.

34 Y. Zhang, D. Li and R. G. Compton, Arsenic(III) Detection with Underpotential Deposition and Anodic Stripping Voltammetry, *ChemElectroChem*, 2021, **8**(19), 3707–3715.

35 S. K. Pal, N. Akhtar and S. K. Ghosh, Determination of arsenic in water using fluorescent ZnO quantum dots, *Anal. Methods*, 2016, **8**(2), 445–452.

36 R. S. Salunke, C. K. Kasar, M. A. Bangar, P. G. Chavan and D. J. Shirale, Electrodeposition of gold nanoparticles decorated single polypyrrole nanowire for arsenic detection in potable water: a chemiresistive sensor device, *J. Mater. Sci.*, 2017, **28**(19), 14672–14677.

37 N. K. Mishra and M. Kidwai, *Green Chemistry: Environmentally Benign Approaches*, BoD–Books on Demand, 2012.

38 K. O. Olumurewa and M. A. Eleruja, Photoelectrical and thermal sensing measurement of spin coated ZnO and ZnO–RGO thin film, *Phys. B*, 2023, **650**, 414588.

39 V. Malyutina-Bronskaya, V. Zalesski, D. Zhyhulin and A. Mudryi, Structural, optical and photoelectric properties of Tb doped ZnO thin films for device applications, *Opt. Mater.*, 2022, **127**, 112305.

40 L. Li, Z. Zhang, J. Wang and P. Yang, Improving photoelectric performance with hydrogen on Al-doped ZnO, *Mater. Chem. Phys.*, 2022, **291**, 126680.

41 J. Wang, H. Yang and P. Yang, Photoelectric properties of 2D ZnO, graphene, silicene materials and their heterostructures, *Composites, Part B*, 2022, **233**, 109645.

42 D. Ahmad, M. Z. Manzoor, R. Kousar, H. H. Somaily, S. A. Buzdar, H. Ullah and Z. Batool, Ternary metal oxide $WO_3 \cdot NiO \cdot ZnO$ nanoparticles and their composite with CNTs for organic dye photocatalytic degradation, *Ceram. Int.*, 2022, **48**, 22269–22277.

43 F. Sanakousar, C. Vidyasagar, V. Jiménez-Pérez and K. Prakash, Recent progress on visible-light-driven metal and non-metal doped ZnO nanostructures for photocatalytic degradation of organic pollutants, *Mater. Sci. Semicond. Process.*, 2022, **140**, 106390.

44 A. Saka, J. L. Tesfaye, L. Gudata, R. Shanmugam, L. P. Dwarampudi, N. Nagaprasad and S. Rajeshkumar, Characterization, and antibacterial activity of ZnO nanoparticles from fresh leaf extracts of Apocynaceae, *Carissa spinarum* L.(Hagamsa), *J. Nanomater.*, 2022, 1–6.

45 S. Soylu, M. Kara, M. Türkmen and B. Şahin, The effect of *Thymus syriacus* plant extract on the main physical and antibacterial activities of ZnO nanoparticles synthesized by SILAR method, *Inorg. Chem. Commun.*, 2022, **135**, 109088.

46 A. C. Badgujar, B. S. Yadav, G. K. Jha and S. R. Dhage, Room temperature sputtered aluminum-doped ZnO thin film transparent electrode for application in solar cells and for low-band-gap optoelectronic devices, *ACS Omega*, 2022, **7**, 14203–14210.

47 Y. Zhao, H. Yang, Y. Xiao and P. Yang, A pathway for ZnO p-type transformation and its performance in solar cells, *Sol. Energy*, 2022, **231**, 889–896.

48 R. D. Chavan, M. Wolska-Pietkiewicz, D. Prochowicz, M. Jędrzejewska, M. M. Tavakoli, P. Yadav and J. Lewiński, Organic Ligand-Free ZnO Quantum Dots for Efficient and Stable Perovskite Solar Cells, *Adv. Funct. Mater.*, 2022, 2205909.

49 E. Alp-Erbay, Nanomaterials Utilized in Food Packaging: State-of-the-Art, *Food Eng. Rev.*, 2022, **14**(4), 629–654.

50 D. Kundu, C. Hazra, A. Chatterjee, A. Chaudhari and S. Mishra, Extracellular biosynthesis of zinc oxide nanoparticles using *Rhodococcus pyridinivorans* NT2: multifunctional textile finishing, biosafety evaluation and *in vitro* drug delivery in colon carcinoma, *J. Photochem. Photobiol., B*, 2014, **140**, 194–204.

51 O. Kalu, J. A. D. Moller and A. R. Rojas, Structural and optical properties of cadmium magnesium zinc oxide (CdMgZnO) nanoparticles synthesized by sol–gel method, *Phys. Lett. A*, 2019, **383**, 1037–1046.

52 Z. Zhuang, Y. Chen, K. Chen, Z. Liu, Z. Guo and X. Huang, *In situ* synthesis of ZnO onto nanoporous gold microelectrode for the electrochemical sensing of arsenic(III) in near-neutral conditions, *Sens. Actuators, B*, 2023, **378**, 133184.

53 S. Singh, S. Khasnabis, A. G. Anil, V. Kumar, T. S. K. Naik, B. Nath and P. C. Ramamurthy, Multifunctional nanohybrid for simultaneous detection and removal of arsenic(III) from aqueous solutions, *Chemosphere*, 2022, **289**, 133101.

54 S. K. Pal, N. Akhtar and S. K. Ghosh, Determination of arsenic in water using fluorescent ZnO quantum dots, *Anal. Methods*, 2016, **8**(2), 445–452.

55 A. Q. Dao, D. M. Nguyen and T. T. T. Toan, Determination of arsenic(III) in water using gold nanorods-modified electrode, *J. Mater. Sci.: Mater. Electron.*, 2021, **32**(23), 27962–27974.

56 A. P. M. Udayan, B. Kachwala, K. G. Karthikeyan and S. Gunasekaran, Ultrathin quasi-hexagonal gold nanostructures for sensing arsenic in tap water, *RSC Adv.*, 2020, **10**(34), 20211–20221.

57 P. N. D. Duoc, N. H. Binh, T. Van Hau, C. T. Thanh, P. Van Trinh, N. V. Tuyen and N. Van Chuc, A novel electrochemical sensor based on double-walled carbon nanotubes and graphene hybrid thin film for arsenic (V) detection, *J. Hazard. Mater.*, 2020, **400**, 123185.

58 A. Karthika, S. Selvarajan, P. Karuppasamy, A. Suganthi and M. Rajarajan, A novel highly efficient and accurate electrochemical detection of poisonous inorganic arsenic(III) ions in water and human blood serum samples based on $SrTiO_3$/β-cyclodextrin composite, *J. Phys. Chem. Solids*, 2019, **127**, 11–18.

59 S. Ismail, N. A. Yusof, J. Abdullah and S. F. Abd Rahman, Development of electrochemical sensor based on silica/gold nanoparticles modified electrode for detection of arsenite, *IEEE Sens. J.*, 2019, **20**(7), 3406–3414.